



UNIVERSITY OF LEEDS

This is a repository copy of *A Cu<sup>2+</sup> complex induces the aggregation of human papillomavirus oncoprotein E6 and stabilizes p53.*

White Rose Research Online URL for this paper:  
<http://eprints.whiterose.ac.uk/134363/>

Version: Accepted Version

---

**Article:**

Kumar, A, Kuhn, LT and Balbach, J (2018) A Cu<sup>2+</sup> complex induces the aggregation of human papillomavirus oncoprotein E6 and stabilizes p53. The FEBS journal. ISSN 1742-464X

<https://doi.org/10.1111/febs.14591>

---

(c) 2018 Federation of European Biochemical Societies. This is the accepted version of the following article: Kumar, A, Kuhn, LT and Balbach, J (2018) A Cu<sup>2+</sup> complex induces the aggregation of human papillomavirus oncoprotein E6 and stabilizes p53. The FEBS journal. ISSN 1742-464X, which has been published in final form at <https://doi.org/10.1111/febs.14591>

**Reuse**

Items deposited in White Rose Research Online are protected by copyright, with all rights reserved unless indicated otherwise. They may be downloaded and/or printed for private study, or other acts as permitted by national copyright laws. The publisher or other rights holders may allow further reproduction and re-use of the full text version. This is indicated by the licence information on the White Rose Research Online record for the item.

**Takedown**

If you consider content in White Rose Research Online to be in breach of UK law, please notify us by emailing [eprints@whiterose.ac.uk](mailto:eprints@whiterose.ac.uk) including the URL of the record and the reason for the withdrawal request.



[eprints@whiterose.ac.uk](mailto:eprints@whiterose.ac.uk)  
<https://eprints.whiterose.ac.uk/>

# Small molecule induces the aggregation of human papillomavirus oncoprotein E6 and stabilizes p53

Amit Kumar<sup>1,2,3\*</sup>, Lars T. Kuhn<sup>1</sup> and Jochen Balbach<sup>2,3\*</sup>

<sup>1</sup> Astbury Centre for Structural Molecular Biology, School of Molecular and Cellular Biology, University of Leeds, Leeds LS2 9JT, UK

<sup>2</sup> Institute of Physics, Biophysics, Martin-Luther-University Halle-Wittenberg, Germany

<sup>3</sup> Institute of Technical Biochemistry e.V., Martin-Luther-University Halle-Wittenberg, Germany

\*Corresponding authors

Amit Kumar, Phone: +44 113 34 37036, E-mail: A.Kumar@leeds.ac.uk

Jochen Balbach, Phone: +49 345 55 28550, E-mail: jochen.balbach@physik.uni-halle.de

## Abstract

Papillomavirus oncoprotein E6 is a critical factor in the modulation of cervical cancer in humans. At the molecular level, formation of the E6-E6AP-p53 ternary complex, which directs p53's degradation, is the key instigator of cancer transforming properties. Herein, a Cu<sup>2+</sup> anthracenyl-terpyridine complex is described which specifically induces the aggregation of E6 in vitro and in cultured cells. For a hijacking mechanism, both E6 and E6AP are required for p53 ubiquitination and degradation. The Cu<sup>2+</sup> complex interacts with E6 at the E6AP and p53 binding sites. We show that E6 function is suppressed by aggregation, rendering it incapable of hijacking p53 and thus increasing its cellular level. Therapeutic treatments of cervical cancer are currently unavailable to infected individuals. We anticipate that this Cu<sup>2+</sup> complex might open up a new therapeutic avenue for the design and development of new chemical entities for the diagnosis and treatment of HPV-induced cancers.

Key words: Human papillomavirus, coordination complex, HPV E6, protein aggregation, p53, NMR

## **Introduction**

High-risk HPV infection is the leading cause of nearly all cases (99.7 %) of cervical cancer [1]. It integrates into the host's DNA and infects the basal cells of cervix, resulting in the production of damaged and disorganized cervical cells. The concomitant loss of function leads to the development of cancer. Over 170 types of HPV are known, of which more than 40 are sexually transmitted. Around 13 high-risk types of HPV are known to cause cervical cancers [2], with types 16 and 18 being the most prevalent, causing over 70 % of cervical cancers [3]. More than 80 % of women are infected with genital HPV at some point in their lives which often leads to cervical cancer [4]. Although HPV infection is widespread, its symptoms are seldom noticeable.

The genome of HPV 16 and 18 is ~8 kb, which is made-up of double-stranded DNA. Of the eight different types of proteins encoded by the HPV genome, only E6 and E7 proteins exhibit cancer inducing properties. These proteins functions include immortalization of primary cell lines, activation of transmembrane signalling and alteration of the cell cycle etc. Thus, E6 and E7 are known to exhibit pleiotropic functions. Thus, E6 and E7 are considered necessary for malignant conversion. The interactions of E6 and E7 with p53 and pRB, respectively, have been suggested to be implicated in the mechanism of inducing tumor formation [5-9]. The E6 protein promotes the formation of a trimeric protein complex composed of E6, p53 and the cellular ubiquitination enzyme E6AP [10, 11]. This stimulates degradation of p53 and thereby promotes unregulated cell proliferation, finally leading to increased tumor cell growth [9]. This explains why very low levels of p53 are observed in cervical carcinoma cell lines [12]. Moreover, E6 can perform its oncogenic activities without the cross-talk of p53 [13, 14]. Discovery of E6 targets is continuous, several have been identified recently. Example include, IRF-3, E6TP1, p300/CBP, ADA3, Gps2 and hMcm7, (transcription and DNA replication

regulatory proteins) and cMyc, FADD, Bak and TNF receptor 1 (apoptosis and immune evasion regulatory molecules). Besides these, E6 also targets proteins included in cell differentiation, cell-cell adhesion, epithelial cell organization, cell polarity and DNA repair [7-9, 13-15].

Recent studies of the structure of an E6/E6AP/p53 complex suggested that ternary complex formation is required for HPV-mediated degradation of p53 [10]. The complex structure also showed that E6 forms a distinct pocket for E6AP and a cleft for p53 binding. Recent experimental evidence using pro-apoptotic peptides and small molecules highlighted that the E6AP binding pocket is druggable [16-18]. Additionally, the p53 binding cleft may represent a second potential drug binding site [10]. Therefore, HPV E6 could be an efficient drug target in order to combat cervical cancer.

Small molecules including coordination complexes are known for their antitumor activities. Cis-platin is a one such example of a coordination complex. Its mechanism of action involves the formation of adducts with DNA, leading to cell death. It is also being developed as a lead molecule against amyotrophic lateral sclerosis based on its interaction with superoxide dismutase [19, 20]. Complexes with other metal ions including  $\text{Cu}^{2+}$  are under intense investigation [21, 22]. Cell toxicity is well known for copper itself, however, its complexes which exhibit several fold better responses are under consideration. Several studies have shown the antiproliferative activity of copper complex exhibited up to several-hundred fold better responses compared to  $\text{Cu}^{2+}$  alone [21, 23-25].

Several of these organometallic complexes have been shown to exhibit antiproliferative, antimicrobial and antifungal activity by adding and incubating them to cultured media. However, the molecular mechanism behind their cytotoxicity remains elusive [26, 27]. In a structure based drug-design, the physico-chemical nature of the molecules often render them

incapable of crossing cell wall/membrane barrier to reach their targets in a complex cellular environment, although they are quite effective binding-partners under in vitro conditions [28]. Thus, small molecules which penetrate the cell and interact with crucial molecules are advantageous [29, 30]. Cell based rational screening identified a  $\text{Cu}^{2+}$  complex which caused E6 to aggregate, we have subsequently explored the molecular mechanism of action. We confirmed that this  $\text{Cu}^{2+}$  complex interacts with the E6 oncoprotein, causes its aggregation inside the cells which is manifested by the formation of granular structures. Only HPV infected cells display such aggregates. Under in vitro conditions, the  $\text{Cu}^{2+}$  complex binds E6 with micromolar affinity and also with those residues forming the E6AP and p53 binding sites. Subsequent self-association forms aggregated structures under in vitro conditions similar to those observed inside the HPV-containing HeLa cells. Eventually, this led to stabilization of p53 inside the cells.

## Results

### **Cu<sup>2+</sup> complex induces aggregation of isolated E6 F47R 4C/4S**

Wild-type oncogenic E6 has a tendency to aggregate under isolated in vitro conditions [31, 32]. Therefore, a soluble construct of E6 (His6-MBP-tev-F47R E6 4C/4S) was expressed and purified via the bacterial-expression system as described previously [32]. For HPV16 E6, we purified the monomeric E6 F47R 4C/4S variant that combines the F47→R47 (F47R) mutation which disrupts the dimerization facilitated by the N-terminal domain ( ) with four mutations at non-conserved cysteines (C80S, C97S, C111S and C140S) preventing disulfide-mediated aggregation [32]. In order to test whether the Cu<sup>2+</sup> complex (stable, water soluble and structurally characterized) can induce the aggregation of E6 F47R 4C/4S in isolation, the complex and ligand were co-incubated for 6 h. Samples were taken out at each hour and analysed by electron microscopy. The results show that E6 F47R 4C/4S aggregates in the presence of the Cu<sup>2+</sup> complex under in vitro conditions and well-defined spherical structures formed at longer times (Figure 1A). The sample, which was incubated for 6 h, was centrifuged at 30,000 rpm and the obtained pellet was washed with buffer and loaded onto SDS-PAGE. The Coomassie brilliant blue-stained gel shows an intense band corresponding to monomeric E6 F47R 4C/4S and additional bands for higher oligomers (Figure 1B) thus confirming that the pelletable material was proteinaceous and sedimented due to the aggregation of E6 F47R 4C/4S. In addition, Cu<sup>2+</sup>-perchlorate or 9-anthracene methanol were used as control molecules. Both did not induce the formation of such aggregates when analysed by EM or SDS-PAGE (Figure 1B ).

Fluorescence correlation spectroscopy (FCS) is a technique well-suited to study the diffusion of proteins and obtain their hydrodynamic radii in solution. E6 F47R 4C/4S has 10 cysteines, of which 8 are involved in forming coordination bonds with zinc, with the remaining two

cysteines free. Therefore, E6 F47R 4C/4S was labelled with the dye Alexa-488 using maleimide chemistry. The  $\text{Cu}^{2+}$  complex-induced aggregation of E6 F47R 4C/4S was monitored for 0 – 6 h doped with 1 % (v/v) Alexa-488-labelled E6 F47R 4C/4S. Analysis of the autocorrelation curves revealed hydrodynamic radii ( $R_H$ ) of 2.1, 2.5, 82.4, 276.8, 366.4, 445.2, and 1128.8 nm after 0, 60, 120, 180, 240, 300 and 360 minutes of incubation, respectively. During the first hour, oligomeric species form which are approximately five times larger than the monomer. After this lag time, the  $\text{Cu}^{2+}$  complex induces the formation of E6 F47R 4C/4S aggregates with increasing size, in good agreement with the EM data. It is notable that  $\text{Cu}^{2+}$ -perchlorate or 9-anthracene methanol have negligible effects on the diffusion of E6 F47R 4C/4S.

Particles with diameters of 40-2000 nm can be analysed by nanoparticle tracking analysis (NTA) [33]. Free form of E6 F47R 4C/4S is not visible under such conditions indicative of the homogeneous monodisperse nature of the sample. A co-incubation of E6 F47R 4C/4S and the  $\text{Cu}^{2+}$  complex for 6 h results in the visualization and quantitation of tracked particles ranging from 13 to >800 nm. At 0 h, or after co-incubation with  $\text{Cu}^{2+}$ -perchlorate or 9-anthracene methanol no particles are visible even after 6 h. The NTA data can be corroborated by using dynamic light scattering (DLS), a complementary technique. Unlike NTA, DLS is able to detect monomeric (<10 nm in radius) as well as aggregated (>10 nm in radius) E6 F47R 4C/4S species. Regularization analysis of the free E6 F47R 4C/4S correlogram gives a single peak with a mean hydrodynamic radius of  $2.3 \pm 0.02$  nm (corresponding to 100 % abundance) expected for a protein of this size and in good agreement with the FCS data. However,  $\text{Cu}^{2+}$ -complex-induced aggregation of E6 F47R 4C/4S after 6 h of co-incubation gives a polydispersity index of over 0.7 indicative of the formation of aggregates over a broad size range. Interestingly, there is no peak corresponding to monomeric protein in the regularization

analysis. It shows three peaks at  $7.89 \pm 1.22$  nm,  $357 \pm 387$  nm and  $10000 \pm 29700$  nm. E6 F47R 4C/4S in the presence of  $\text{Cu}^{2+}$ -perchlorate or 9-anthracene methanol gives a single peak at  $2.3 \pm 0.1$  nm and  $2.4 \pm 0.3$  nm, respectively, after 6 h of co-incubation.

### **Interactions of the $\text{Cu}^{2+}$ complex with E6 F47R 4C/4S**

Next, the interactions of the  $\text{Cu}^{2+}$  complex with E6 F47R 4C/4S were probed by fluorescence spectroscopy. E6 F47R 4C/4S features one tryptophan at position 132 which acts as a highly sensitive fluorescence probe for interaction studies. A symptomatic decrease in fluorescence intensity was observed upon addition of the  $\text{Cu}^{2+}$  complex to protein (Figure 2A), yielding a  $K_d$  of  $1.1 \pm 0.06$   $\mu\text{M}$  and a stoichiometry of 1:2. Thus, at least two molecules of  $\text{Cu}^{2+}$  complex bind to E6 F47R 4C/4S. Such binding is expected from organic molecules bearing a hydrophobic moiety. The titration with  $\text{Cu}^{2+}$ -perchlorate did not result in a considerable decrease in fluorescence intensity. The binding of E6 F47R 4C/4S to 9-anthracene methanol yielded a  $K_d$  of 4.95 mM indicating that both the Cu-metal centre and the organic moiety are required for effective binding.

E6 F47R 4C/4S exhibits a characteristic circular dichroism spectrum expected from the NMR/X-ray structure [10, 32] of the  $\alpha/\beta$ -protein. Titration with the  $\text{Cu}^{2+}$  complex showed a gradual loss of negative ellipticity at 210 and 220 nm together with a decrease at 195 nm. This indicates that E6 F47R 4C/4S undergoes conformational changes of some secondary structure elements towards a disordered form. Again,  $\text{Cu}^{2+}$ -perchlorate or 9-anthracene methanol did not induce significant conformational changes.

### **$\text{Cu}^{2+}$ complex induces intra-cellular aggregation of E6**

In order to test whether the  $\text{Cu}^{2+}$  complex induces the aggregation of E6 inside the cell, HPV-containing HeLa cells were co-incubated. With the molecules, HPV-infected HeLa cells showed spherical aggregated structures within 2 h of incubation. Similar spherical structures were observed previously, but, their origin was unclear [23]. These spherical structures give rise to blue fluorescence when observed under UV light (334 nm) (Figures 3 A and B). The HeLa cells showed an  $\text{IC}_{50}$  (concentration at which cells showed 50% viability) value for cell viability of  $1.03 \pm 0.03 \mu\text{M}$   $\text{Cu}^{2+}$  complex (Figure 3 C). Subsequently, rational screening of cells infected with HPV (CaSki, HeLa, SiHa and ME 180) or not (HepG2, MCF7, H1229, U2OS, and HEK 293) showed direct correlation of  $\text{IC}_{50}$  and involvement of HPV (Figure 3 C). Accordingly, CaSki (60-600 copies/cell), HeLa (10-50 copies/cell), SiHa (1-2 copies/cell) and ME180 (HPV-68) showed  $\text{IC}_{50}$  value of  $0.7 \pm 0.02 \mu\text{M}$ ,  $1.03 \pm 0.03 \mu\text{M}$ ,  $4.1 \pm 0.7 \mu\text{M}$ , and  $5.20 \pm 0.4 \mu\text{M}$ , respectively. The other cell lines (non HPV-infected) showed similar toxicity against  $\text{Cu}^{2+}$  complex, with an  $\text{IC}_{50}$  range between 5 – 6  $\mu\text{M}$  (Figure 3 C). Western blotting confirmed that the spherical structures are aggregated species of E6. Untreated HeLa cells showed similar levels of E6 in the soluble fraction and the cells pellet in lysed cells (Figure 3D, lanes 1 and 2). In contrast, when the cells were treated with the  $\text{Cu}^{2+}$  complex, the majority of the E6 protein was observed in the cell pelleted fraction (Figure 3D, lanes 3 and 4).

Although these experiments provided sufficient evidence of  $\text{Cu}^{2+}$  complex-induced aggregation of E6, it is well known that wild-type E6 aggregates in isolation [31, 32]. Therefore, the pellet observed (Figure 3D, lane 4) could be simply induced by cell opening (Figure 3D, lane 2). To further confirm E6 aggregation induced by the  $\text{Cu}^{2+}$  complex, soluble E6 F47R 4C/4S was fused with green fluorescence protein (GFP) and sub-cloned into the pFLAG vector for mammalian cell expression. This construct was transiently transfected into MCF-7 cells. Note that MCF-7 cells are HPV negative and therefore contain no endogenous

E6. The green fluorescence of GFP-E6 F47R 4C/4S inside MCF-7 cells when excited at 488 nm was broadly distributed throughout the cytoplasm (Figures 3 E and F). Subsequently, these cells were co-incubated with the  $\text{Cu}^{2+}$  complex which, after 2 h of incubation, showed spherical aggregates inside the transfected HCF-7 cells (tMCF-7) (Figures 3 G and H). The transfected cells without  $\text{Cu}^{2+}$  complex treatment showed maximum expression of GFP-E6 F47R 4C/4S in the soluble fraction (Figure 3 I, lane 1 and 2). However, most of the GFP-E6 F47R 4C/4S was seen in the pellet when transfected MCF-7 cells were co-incubated with the  $\text{Cu}^{2+}$  complex (Figure 3 I, lane 3 and 4). The transfected cells showed a three-fold lower  $\text{IC}_{50}$  value ( $1.88 \pm 0.05 \mu\text{M}$ ) compared to the non-transfected MCF-7 cells ( $5.94 \pm 0.5 \mu\text{M}$ ) (Figure 3 C) by the MTT cell viability assay. These results confirm that granular structures inside the cells are formed due to the aggregation of E6 induced by the  $\text{Cu}^{2+}$  complex. Neither,  $\text{Cu}^{2+}$ -perchlorate nor 9-anthracene methanol induce such spherical aggregated structures in HeLa, MCF-7, or transfected MCF-7 cells transiently expressing GFP-E6 F47R 4C/4S .

### **p53 hijacking by E6 can be relieved by the $\text{Cu}^{2+}$ complex**

p53 is a transcription factor that plays a key role in regulating cell cycle progression, DNA repair and apoptosis [34]. However, p53 function is masked by E6 in HPV-infected cells (e.g. cervical cancer cells [35]) where p53 degradation is a hallmark activity of the HPV E6 protein [6-11, 13]. Therefore, we hypothesize that, if we could disrupt E6/E6AP/p53 complex formation e.g. by aggregating E6 in the presence of the  $\text{Cu}^{2+}$  complex, p53 should not degrade and its expression will be stabilized. Western blot analyses show low expression of p53 in untreated HeLa cells as expected due to the hijacking nature of E6 (Figure 4A, lane 1). In doing so, E6 interacts with the LxxLL motif of E6AP, yielding the E6/E6AP heterodimer [10, 11]. This heterodimer recruits and degrades p53 via the ubiquitin-mediated degradation pathways [6-13]. However, in  $\text{Cu}^{2+}$  complex treated cells, p53 expression is upregulated several fold

(Figure 4A, lane 2) suggesting that E6 function is suppressed, most probably by its aggregation. Also, neither E6 nor E6AP are independently capable of recruiting p53 for degradation [36, 37]. Other HPV E6 containing cell line, i.e. CaSki, showed similar p53 stabilization when treated with the Cu<sup>2+</sup> complex (Figure 4A). Additionally, treated cervical cancer cells showed nuclear fragmentation after 48 h of incubation (Figure 4B-G). FACS analysis showed a 55 % and 56 % increase in apoptotic peak in HeLa and CaSki cells, respectively, a clear indication of apoptotic cell death induced by the Cu<sup>2+</sup> complex. In control MCF-7 cells lacking E6, no change in p53 expression or nuclear fragmentation after Cu<sup>2+</sup> complex treatment was observed (Figure 4A, F and G). Taken together, these results suggest that the Cu<sup>2+</sup> complex induces the apoptotic cell death via the p53 mediated pathway.

Next, we evaluated the residue-based interactions of the Cu<sup>2+</sup> complex with E6 F47R 4C/4S, which might be involved in disrupting the E6/E6AP/p53 ternary complex and/or inducing aggregation, by NMR spectroscopy [38-42]. The recent E6 F47R 4C/4S/E6AP/p53-core ternary complex structure suggested that the E6-p53 interface can be sub-divided into three regions [10, 32]. E6 F47R 4C/4S residues at sub-interface I include: Met1-Arg8, Arg10, Lys11, Gln14 and Glu18; at sub-interface II Ile23, His24, Tyr43, Asp44, Phe47, and Asp49, and at sub-interface III; Leu100 and Pro112. The E18A/R point mutation of E6 impaired E6/E6AP/p53 ternary complex assembly, while D44R and D49A substitutions hindered p53 degradation in addition to complex assembly [10]. After addition of the Cu<sup>2+</sup> complex (Figure 4H, I and 5), the NMR intensity of these interface residues revealed almost complete signal loss for Glu18, Asp44 and Asp49 and significant intensity decreases for Glu7, Arg8, Arg10, Ile23, and R47 (marked red in Figure 4 H and I), while residues Met1-Gln6, Lys11, Gln14, His24, Tyr43 and Leu100 remain almost unaffected. NMR intensities decreased for

those residues, which are in close proximity to the paramagnetic  $\text{Cu}^{2+}$  moiety, because of paramagnetic relaxation enhancement [19, 29].

E6 possesses a conserved LxxLL binding pocket formed by residues from the N- and C-terminal domains (denoted as E6N and E6C in Figure 4I) also harbouring the Zn-binding site and the linking helix. Val31, Tyr32, Leu50, Cys51, Val53, Val62, Leu67, Tyr70, Ile73 and Leu100 of E6 contribute to the LxxLL binding pocket [10, 11]. NMR titration shows that the intensities of Val31, Leu50, Cys51, Val53 and Ile73 significantly reduced upon addition of the  $\text{Cu}^{2+}$  complex (marked in magenta in Figure 4 H and I). Thus, various key residues in the N-terminal domain of E6 F47R 4C/4S indicate that the  $\text{Cu}^{2+}$  complex can compete with p53 and E6AP binding. In addition, the NMR titration analysis of the whole E6 F47R 4C/4S sequence showed that the intensity of many other residues from both the N- and C-terminal domain significantly decreased (Figure 5). We anticipate that the local unfolding [43] of E6 F47R 4C/4S upon  $\text{Cu}^{2+}$  complex binding detected by CD spectroscopy might correspond to these residues, which are then responsible for inducing E6 F47R 4C/4S aggregation.

## Discussion

Gardasil and Cervarix are the marketed HPV vaccines offering preventive care to uninfected humans [44, 45]. However, at present, therapeutic treatments are not available to infected individuals. Additionally, these vaccines are expensive and the overall five year treatment rate is ~90 % for cervical cancer, reducing sharply to 15 % if the cancer has spread to other organs (according to the American Cancer Society). We demonstrated that a complex of  $\text{Cu}^{2+}$  and anthracenyl-terpyridine showed sub-micro-molar inhibition of various cervical cancer cell lines. Their  $\text{IC}_{50}$  values showed a clear dependency on the number of HPV copies present in the cancer cell lines and exhibited granulated structures inside cells. We proposed that the  $\text{Cu}^{2+}$  complex induces aggregation of HPV-E6 inside cells, eventually causing apoptosis of HPV-infected cells [23]. As p53 expression levels are quite low in HPV-containing tumor cells, due to E6-directed degradation, many therapeutic strategies have been focused on blocking E6 function, thereby stabilizing p53. An increase in the cellular p53 level and concomitant suppression of tumor growth has been achieved in both tissue culture and animal models using RNAi or antisense oligo-deoxy-nucleotides [46, 47]. Recently reported crystal structures of the ternary complex [10] suggested that another approach is to disrupt the interactions of the E6-E6AP or E6-p53 heterodimer, inducing cell cycle arrest or apoptosis by increasing p53 levels in the infected cells. Several inhibitors such as Pitx2a protein inhibitor [48],  $\alpha$ -helical peptides [49, 50] and intrabodies [51] have been developed, however, all of these show modest activity. An alternate way is to develop small molecules which exhibit the unique phenomenon of nullifying the E6 hijacking function and thus stabilizing the cellular p53 level. The  $\text{Cu}^{2+}$  complex described in the present study exhibits these features by aggregating E6 in vitro and stabilizing cellular levels of p53.

We tested various other small molecules (such as acid fuchsin, acridine orange, fast green FCF, benzimidazole, thioflavin T., vanillin etc) to determine whether or not they can induce E6 F47R 4C/4S aggregation under in vitro conditions. None of these generated observable E6 F47R 4C/4S aggregates. Additionally, previous studies about inhibitors developed to disrupt the E6 ternary complex, never reported aggregation of E6 under any of the experimental conditions tested. These studies include a high throughput screen of flavonoids disrupting HPV-16 E6 function [16], the screening of over 88,000 diverse small molecules as HPV E6 inhibitors [17], the small inhibitory peptides [18], chimeric proteins [52], the Pitx2a protein inhibitor [48],  $\alpha$ -helical peptides [49, 50], and intrabodies [51] to name but a few. We also tested whether the  $\text{Cu}^{2+}$  complex induces aggregation of proteins other than E6 F47R 4C/4S. Although we chose a diverse set of proteins including Kti11, a protein which coordinate  $\text{Zn}^{2+}$  through four cysteine residues [42], or a disulfide bonds rich protein (HSA), none showed formation of well-defined spherical aggregates. Therefore we anticipate that inducing the E6 F47R 4C/4S aggregation phenomenon by the  $\text{Cu}^{2+}$  complex is rather specific.

The aggregates formed by co-incubation of E6 F47R 4C/4S and the  $\text{Cu}^{2+}$  complex are well-defined, round in shape and amorphous in nature. FCS, electron microscopy and dynamic light scattering analyses suggest a gradual increase in the size of the aggregates with time up to 1  $\mu\text{m}$  in diameter. The proteinaceous nature of the aggregate was confirmed by SDS-PAGE. An NMR titration with the  $\text{Cu}^{2+}$  complex revealed the E6 F47R 4C/4S residues sensing binding (Figure 5). In vitro dimerization of E6 occurs via the N-terminal domain [32] and the majority of residues at the dimer interface (Ile23, Arg39, Tyr43, Asp44, Ala46, and Phe47) are also involved in  $\text{Cu}^{2+}$  binding (Figure 5A). Note that Phe47 was mutated to Arg in E6 F47R 4C/4S to increase the solubility and that mutations of the dimer interface disrupt E6 self-association and inactivate E6-mediated p53 degradation [32]. We suggest that the  $\text{Cu}^{2+}$  complex overrides

the solubility promotion of Arg47 leading to E6 aggregates. We cannot distinguish from the data presented here whether disruption of the dimerization or the loss of soluble E6 protein, increases p53 levels in vivo upon incubation with the Cu<sup>2+</sup> complex. Also, we are unable to rule out the possibility that the Cu<sup>2+</sup> complex may interact with other cellular proteins.

E6 F47R 4C/4S binds two Cu<sup>2+</sup> complexes with micromolar affinity ( $K_d = 1 \mu\text{M}$ ). Several residues affected by this binding are also involved in E6AP and p53 binding (Figure 4H and I). Additionally, Cu-perchlorate or 9-anthracene methanol could not establish such residues specific interactions. Therefore, we propose that the Cu<sup>2+</sup> complex can compete with p53 hijacking given that the in vitro  $K_d$  between E6 F47R 4C/4S and the p53 core is within the same range (22  $\mu\text{M}$  according to [10]). Additionally, the Cu<sup>2+</sup> complex interacts with four residues of E6 F47R 4C/4S (V32, L50, V53, I73), which facilitate E6AP binding (Figures 4 H and I). Again we propose that a competition with E6AP is feasible because the E6 F47R 4C/4S/E6AP interaction is in the low micromolar range [18].

In summary, we have shown the aggregation of HPV oncoprotein E6 in vitro and inside cells, and that this phenomenon is exclusively induced by the Cu<sup>2+</sup> complex, leading to increased p53 levels thereby shortening life-time of HPV-infected cells by inducing apoptosis. We anticipate that the Cu<sup>2+</sup> complex described here might lead to the development of drugs which specifically target E6 in cancer cells and combat HPV-mediated infections.

## **Experimental section**

### **Protein expression and purification**

The plasmid corresponding to the DNA sequences of HVP 16 E6 F47R E6 4C/4S was cloned in the NcoI and KpnI sites of the pETM-41 vector containing an N-terminal His<sub>6</sub>-MBP tag followed by a TEV cleavage site. This plasmid was provided by Dr. Gilles Travé, IGBMC, France. F47R E6 4C/4S was purified following the previously reported method [32]. In brief, pETM-41 carrying the gene of F47R E6 4C/4S was transformed into the E. coli BL21(DE3) cells containing kanamycin as the selection antibiotic. These cells were grown in Luria-Bertani media at 37 °C followed by induction with IPTG and further growth for 17 h at 15 °C. The MBP-E6 F47R 4C/4S was purified from the soluble fraction using amylose affinity chromatography. The fused protein was cleaved by TEV protease and further purified by S75 gel filtration chromatography. The purity of the protein was analysed on 12 % SDS-PAGE.

### **Protein aggregation and electron microscopy**

E6 F47R 4C/4S and Cu<sup>2+</sup> complex were mixed in a 1:2 ratio (20:40 μM) and incubated at room temperature in 20 mM sodium phosphate buffer (pH 6.8), 200 mM NaCl and 2 mM DTT. Samples were taken out at 0, 30, 60, 120, 180, 240, 300 and 360 minutes. EM grids were immediately prepared by pipetting the mixture onto a Formvar carbon-coated copper grid. The grids were washed and stained with 25 μl of 2% (w/v) uranyl acetate. The grids were examined using a Zeiss 900 transmission electron microscope operated at an acceleration voltage of 80 kV. The Cu<sup>2+</sup> complex was dissolved in dimethyl sulfoxide (DMSO) and further diluted for experiments. The final concentration of DMSO was < 1 % in any experiment.

The small molecule screening was performed in 20 mM sodium phosphate buffer (pH 6.8), 200 mM NaCl and 2 mM DTT. In these experiments E6 F47R 4C/4S and small molecule were

mixed in a 1:2 ratio of protein:small molecules (20:40  $\mu\text{M}$ ). The protein screening was carried out in 20 mM sodium phosphate buffer (pH 6.8), 200 mM NaCl and 2 mM DTT. Here, the protein solution was mixed with the  $\text{Cu}^{2+}$  complex in a 1:2 mol:mol ratio (protein: $\text{Cu}^{2+}$  complex). The mixture was incubated at room temperature for 6 h and EM grids were prepared as described above.

### **Fluorescence correlation spectroscopy**

Two of the E6 F47R 4C/4S cysteines are available to be labelled using maleimide chemistry. These two cysteine residues in E6 F47R 4C/4S allow site-specific derivatisation using a sulfhydryl reactive fluorophore (Alexa Fluor 488 C5 Maleimide, Molecular Probes). E6 F47R 4C/4S at 50  $\mu\text{M}$  solution (20 mM sodium phosphate buffer (pH 7), 200 mM NaCl) was mixed 1:10 (mol:mol) with Alexa Fluor 488 and allowed to conjugate for 4 h at room temperature. Unreacted dye was then separated from the E6 F47R 4C/4S using a Superdex peptide column (10/300 GL, GE Healthcare). For the aggregation assay, 20  $\mu\text{l}$  (of 20  $\mu\text{M}$ ) of labelled E6 F47R 4C/4S was mixed with 20  $\mu\text{M}$  of unlabelled E6 F47R 4C/4S in 20 mM sodium phosphate buffer (pH 6.8), 200 mM NaCl and 2 mM DTT. The  $\text{Cu}^{2+}$  complex at 40  $\mu\text{M}$  was mixed with this doped mixture. The proteins and  $\text{Cu}^{2+}$  complex were mixed in such a way to give the final concentration identical in 200  $\mu\text{l}$  solution. FCS correlograms were recorded at 0, 30, 60, 120, 180, 240, 300 and 360 minutes on a home-built FCS setup equipped with a Carl Zeiss objective lens with 1.45 numerical apertures and a working distance of 0.11 mm. A green laser (power of 1 mW) was used for recording the data with confocal volume of 1 fL. Averages of 10 successive scans were acquired for a single correlogram. The data were analysed using MATLAB scripts.

### **Fluorescence spectroscopy**

The fluorescence experiments were carried out in 20 mM sodium phosphate buffer (pH 6.8), 200 mM NaCl and 2 mM DTT at 5  $\mu\text{M}$  E6 F47R 4C/4S on a Jasco FP6500. The samples were

excited at 280 nm. In a titration experiment, 4  $\mu\text{M}$  of  $\text{Cu}^{2+}$  complex was added and spectra were recorded after each addition. A blank titration was reference, using  $\text{Cu}^{2+}$  complex alone in buffer, and these spectral traces were subtracted from the main titration data.

Fluorescence data were analyzed according to the following equation:

$$Q = Q_{\max} - \left( Q_{\max} \left( \frac{\left( (P + nL_1 + K_D) - \sqrt{(P + nL_1 + K_D)^2 - 4PnL_1} \right)}{2P} \right) \right) + mL_1 \quad (1)$$

with  $P = (P_0 / (V_0 + L))V_0$  and  $L_1 = (L_0 / (V_0 + L))L$  and  $Q$  – fluorescence intensity,  $P$  – protein concentration,  $L$  – ligand concentration,  $V$  – volume,  $n$  – binding sites and subscript 0 – indicates start point.

### **CD spectroscopy**

CD titration experiments were carried out in 20 mM sodium phosphate buffer (pH 6.8), 200 mM NaCl and 2 mM DTT at 15  $\mu\text{M}$  E6 F47R 4C/4S. In a titration experiment 10  $\mu\text{M}$  of the  $\text{Cu}^{2+}$  complex was added at each time. Final spectra represented are the average of four successive scans. A blank titration containing only the  $\text{Cu}^{2+}$  complex was subtracted from the spectra from the main titration experiment. CD spectra were recorded on a Jasco-J810 spectropolarimeter with a scan speed of 20 nm/min using 1 mm path length cuvette.

### **Dynamic Light Scattering (DLS)**

A 1:2 ratio (20:40  $\mu\text{M}$ ) of E6 F47R 4C/4S and  $\text{Cu}^{2+}$  complex were mixed and incubated at room temperature in 20 mM sodium phosphate buffer (pH 6.8), 200 mM NaCl and 2 mM DTT for 6 h.  $\text{Cu}^{2+}$ -perchlorate or 9-anthracene methanol were also incubated under the same conditions. After 6 h incubation time, 300  $\mu\text{L}$  samples were injected into a Wyatt miniDawnTreos® system (equipped with an additional DLS detector). Filtered (0.22  $\mu\text{m}$ ) and de-gassed buffer was used to obtain 5 minute baselines before and after sample injection. The

flow cell was cleaned after each run using 1 mL of 1 M nitric acid followed by 2 ml each of H<sub>2</sub>O and buffer. Data analysis was performed on a three minute sample window using Astra 6.0.3 software by the methods of regularization [53] and cumulants analysis [54]. Cumulants analysis provided the Z-average radius ( $z$ ) and standard deviation ( $\sigma$ ) of the solution [54]. The polydispersity index (PDI) was calculated using the following equation:

$$PDI = \left( \frac{\sigma^2}{z^2} \right)$$

### **Nanoparticle Tracking Analysis (NTA)**

Nanoparticle tracking analysis was performed on the 1:2 ratio of Cu<sup>2+</sup> complex:E6 F47R 4C/4S which was incubated for 6 h at room temperature. The same conditions were used in the case of Cu<sup>2+</sup>-perchlorate or 9-anthracene methanol. A Nanosight® LM10 (Malvern Instruments) equipped with a 642 nm laser was cleaned with 70 % ethanol and left to dry. 300 µl of samples were injected in the instrument and three 90 second videos were recorded. The data was analyzed and averaged in the software for each sample. The instrument was set at screen gain = 1, detection threshold = 10 nm, T = 22 °C, viscosity = 0.95 cP and camera brightness = 10-16 to minimise background noise.

### **NMR experiments**

For uniform protein <sup>15</sup>N isotope labelling M9 minimal media supplemented with <sup>15</sup>N NH<sub>4</sub>Cl was used. E6 F47R 4C/4S was purified as described in the previous section. NMR experiments were carried out at 50 µM protein concentration in 20 mM sodium phosphate buffer (pH 6.8), 200 mM NaCl and 2 mM DTT. The Cu<sup>2+</sup> complex was added until no further changes in cross-peak intensities were observed. NMR spectra were recorded with a Bruker 800 MHz Avance III spectrometer equipped with a CP-TCI cryoprobe at 25 °C. Spectra were processed using the programs NMRPipe and NMR Draw. The spectrum corresponding to the 1:2 ratio of E6 F47R

4C/4S to Cu<sup>2+</sup> complex was analysed. Previously assigned NMR resonances [32] were used for data analysis. Cu<sup>2+</sup>-perchlorate or 9-anthracene methanol was mixed with E6 F47R 4C/4S at 1:2 ratio and spectrum was recorded as described above.

### **Cell culture**

Cervical carcinoma cells (HeLa) and breast cancer cells (MCF-7) were cultured in DMEM, whilst CaSki (cervical carcinoma cells) were cultured in RPMI media supplemented with 10 % heat inactivated (56 °C for 30 min) fetal bovine serum (FBS) at 37 °C in a humidified chamber with 5 % CO<sub>2</sub>.

### **Cell viability assay**

Cell viability was determined by a methylthiazole tetrazolium (MTT) assay. HeLa, MCF-7 or transfected MCF-7 cells were co-incubated with increasing amounts of the Cu<sup>2+</sup> complex (0 – 15 µM). After 48 h of incubation, 50 µl of MTT (1 mg/ml) was added and further incubated for 4 h at 37 °C. Thereafter, 100 µl of DMSO was added and absorbance was recorded at 570 nm using 630 nm as a reference filter. The cells measured without the Cu<sup>2+</sup> complex were considered as having 100 % cell viability. The experiments were performed in triplicates and repeated three times. In the control experiment cells were treated with 15 µM of Cu<sup>2+</sup>-perchlorate or 9-anthracene methanol. For nuclear fragmentation experiments cells were tested at IC<sub>50</sub> (HeLa and CaSki cells at 1 µM and MCF-7 cells at 6 µM) and incubated for 48 h.

### **Transfection experiment**

The MCF-7 cells were transfected by Lipofectamine2000 (Invitrogen) following the manufacturer's instructions. Semi-confluent (80–90%) MCF-7 cells were transfected with 2 µg of pFLAG-GFP-E6 F47R 4C/4S. As an internal control, 0.5 µg of pEGFP1 plasmid was

added to assess the transfection efficiency. The final DNA amount was adjusted to 6  $\mu\text{g}$  using the pCDNA plasmid as carrier DNA. This DNA mixture was added to Lipofectamine2000 (diluted Opti-MEM medium). This mixture was incubated at room temperature for 45 min to allow Lipofectamine2000-DNA complex formation. The Lipofectamine2000-DNA complex was added drop wise to the MCF-7 cells and mixed gently.

### **Western blot analysis**

For the Western blot analysis, the cells were treated at the  $\text{IC}_{50}$  concentration (HeLa and CaSki cells at 1  $\mu\text{M}$  and transfected MCF-7 cells at 2  $\mu\text{M}$ ) and incubated for 48 h. Cells were washed with ice cold phosphate buffered saline and lysed with lysis buffer (50 mM Tris-Cl, pH 7.5, with 120 mM NaCl, 10 mM NaF, 10 mM sodium pyrophosphate, 2 mM EDTA, 1 mM  $\text{Na}_3\text{VO}_4$ , 1 mM PMSF, 1% NP-40 and protease inhibitor cocktail). Fifty  $\mu\text{g}$  of heated proteins (95  $^{\circ}\text{C}$  for 10 min) in 1x SDS-loading buffer (50 mM Tris-Cl (pH 6.8), 2.5%  $\beta$ -mercaptoethanol, 2% SDS, 0.1% bromophenol blue, 10% glycerol) was resolved on SDS-PAGE. The proteins were transferred onto a nitrocellulose membrane. The cut strips of membrane corresponding with the appropriate protein size, e.g., E6/E6 F47R 4C/4S ~19 kDa, GFP-E6 F47R 4C/4S ~46 kDa, p53 ~43 kDa and GAPDH ~35 kDa, were washed and incubated with 1:1000 dilutions of E6, GFP, p53 or GAPDH antibodies, respectively. After washing, the membranes were then incubated with 1:2,000 dilutions of HRP-linked secondary antibodies. The HRP activity was detected by chemiluminescence. In these experiments, GAPDH served as loading control. The antibodies were purchased from AbCam, Cambridge, UK.

### **Author contribution**

AK and JB designed the experiments. AK and LTK performed the experiments. AK, LTK and JB analysed the data and wrote the manuscript.

### **Acknowledgments**

We thank Prof. C P Rao for providing the Cu<sup>2+</sup> anthracenyl-terpyridine complex (covered under patent: IPA Application No. 1819/MUM/2011. O/ref: 2866-2011/KG/SKK/cr). The soluble construct of E6 was kindly provided by Dr. Gilles Travé, IGBMC, France. Leon F. Willis is greatly acknowledged for his careful reading of the manuscript. This work has been supported by grants from the DFG (GRK 1026, SFB TRR102), the BMBF (ProNet-T3), the state Sachsen-Anhalt (Exzellenznetzwerk Biowissenschaften), and ERDF by the EU.

## References:

1. Walboomers, J. M., Jacobs, M. V., Manos, M. M., Bosch, F. X., Kummer, J. A., Shah, K. V., Snijders, P. J., Peto, J., Meijer, C. J. & Munoz, N. (1999) Human papillomavirus is a necessary cause of invasive cervical cancer worldwide, *J Pathol.* **189**, 12-19.
2. Li, N., Franceschi, S., Howell-Jones, R., Snijders, P. J. & Clifford, G. M. (2011) Human papillomavirus type distribution in 30,848 invasive cervical cancers worldwide: Variation by geographical region, histological type and year of publication, *Int J Cancer.* **128**, 927-935.
3. Bosch, F. X., Burchell, A. N., Schiffman, M., Giuliano, A. R., de Sanjose, S., Bruni, L., Tortolero-Luna, G., Kjaer, S. K. & Munoz, N. (2008) Epidemiology and natural history of human papillomavirus infections and type-specific implications in cervical neoplasia, *Vaccine.* **26 Suppl 10**, K1-16.
4. Muñoz, N., Hernandez-Suarez, G., Mendez, F., Molano, M., Posso, H., Moreno, V., Murillo, R., Ronderos, M., Meijer, C. & Munoz, A. (2009) Persistence of HPV infection and risk of high-grade cervical intraepithelial neoplasia in a cohort of Colombian women, *Br J Cancer.* **100**, 1184-1190.
5. Boyer, S. N., Wazer, D. E. & Band, V. (1996) E7 protein of human papilloma virus-16 induces degradation of retinoblastoma protein through the ubiquitin-proteasome pathway, *Cancer Res.* **56**, 4620-4624.
6. Scheffner, M., Huibregtse, J. M., Vierstra, R. D. & Howley, P. M. (1993) The HPV-16 E6 and E6-AP complex functions as a ubiquitin-protein ligase in the ubiquitination of p53, *Cell.* **75**, 495-505.
7. Gross-Mesilaty, S., Reinstein, E., Bercovich, B., Tobias, K. E., Schwartz, A. L., Kahana, C. & Ciechanover, A. (1998) Basal and human papillomavirus E6 oncoprotein-induced

degradation of Myc proteins by the ubiquitin pathway, *Proc Natl Acad Sci USA*. **95**, 8058-8063.

8. Kesis, T. D., Slebos, R. J., Nelson, W. G., Kastan, M. B., Plunkett, B. S., Han, S. M., Lorincz, A. T., Hedrick, L. & Cho, K. R. (1993) Human papillomavirus 16 E6 expression disrupts the p53-mediated cellular response to DNA damage, *Proc Natl Acad Sci USA*. **90**, 3988-3992.

9. Mortensen, F., Schneider, D., Barbic, T., Sladewska-Marquardt, A., Kuhnle, S., Marx, A. & Scheffner, M. (2015) Role of ubiquitin and the HPV E6 oncoprotein in E6AP-mediated ubiquitination, *Proc Natl Acad Sci USA*. **112**, 9872-9877.

10. Martinez-Zapien, D., Ruiz, F. X., Poirson, J., Mitschler, A., Ramirez, J., Forster, A., Cousido-Siah, A., Masson, M., Vande Pol, S., Podjarny, A., Trave, G. & Zanier, K. (2016) Structure of the E6/E6AP/p53 complex required for HPV-mediated degradation of p53, *Nature*. **529**, 541-545.

11. Zanier, K., Charbonnier, S., Sidi, A. O., McEwen, A. G., Ferrario, M. G., Poussin-Courmontagne, P., Cura, V., Brimer, N., Babah, K. O., Ansari, T., Muller, I., Stote, R. H., Cavarelli, J., Vande Pol, S. & Trave, G. (2013) Structural basis for hijacking of cellular LxxLL motifs by papillomavirus E6 oncoproteins, *Science*. **339**, 694-698.

12. Münger, K., Scheffner, M., Huibregtse, J. M. & Howley, P. M. (1992) Interactions of HPV E6 and E7 oncoproteins with tumour suppressor gene products, *Cancer Surv*. **12**, 197-217.

13. Crook, T., Tidy, J. A. & Vousden, K. H. (1991) Degradation of p53 can be targeted by HPV E6 sequences distinct from those required for p53 binding and trans-activation, *Cell*. **67**, 547-556.

14. Yim, E. K. & Park, J. S. (2005) The role of HPV E6 and E7 oncoproteins in HPV-associated cervical carcinogenesis, *Cancer Res Treat*. **37**, 319-324.

15. Filippova, M., Parkhurst, L. & Duerksen-Hughes, P. J. (2004) The human papillomavirus E6 protein binds to Fas-associated death domain and protects cells from Fas-triggered apoptosis, *J Biol Chem.* **279**, 25729-25744.
16. Cherry, J. J., Rietz, A., Malinkevich, A., Liu, Y., Xie, M., Bartolowits, M., Davisson, V. J., Baleja, J. D. & Androphy, E. J. (2013) Structure based identification and characterization of flavonoids that disrupt human papillomavirus-16 E6 function, *PloS one.* **8**, e84506.
17. Malecka, K. A., Fera, D., Schultz, D. C., Hodawadekar, S., Reichman, M., Donover, P. S., Murphy, M. E. & Marmorstein, R. (2014) Identification and characterization of small molecule human papillomavirus E6 inhibitors, *ACS Chem Biol.* **9**, 1603-1612.
18. Zanier, K., Stutz, C., Kintscher, S., Reinz, E., Sehr, P., Bulkescher, J., Hoppe-Seyler, K., Trave, G. & Hoppe-Seyler, F. (2014) The E6AP binding pocket of the HPV16 E6 oncoprotein provides a docking site for a small inhibitory peptide unrelated to E6AP, indicating druggability of E6, *PloS one.* **9**, e112514.
19. Banci, L., Bertini, I., Blazevits, O., Calderone, V., Cantini, F., Mao, J., Trapananti, A., Vieru, M., Amori, I., Cozzolino, M. & Carri, M. T. (2012) Interaction of cisplatin with human superoxide dismutase, *J Am Chem Soc.* **134**, 7009-7014.
20. Wang, D. & Lippard, S. J. (2005) Cellular processing of platinum anticancer drugs, *Nat Rev Drug Discov.* **4**, 307-320.
21. Santini, C., Pellei, M., Gandin, V., Porchia, M., Tisato, F. & Marzano, C. (2014) Advances in copper complexes as anticancer agents, *Chem Rev.* **114**, 815-862.
22. Medici, S., Peana, M., Nurchi, V. M., Lachowicz, J. I., Crisponi, G. & Zoroddu, M. A. (2015) Noble metals in medicine: Latest advances, *Coord Chem Rev.* **284**, 329–350.
23. Kumar, A., Chinta, J. P., Ajay, A. K., Bhat, M. K. & Rao, C. P. (2011) Synthesis, characterization, plasmid cleavage and cytotoxicity of cancer cells by a copper(II) complex of anthracenyl-terpyridine, *Dalton Trans.* **40**, 10865-10872.

24. Kumar, A., Mitra, A., Ajay, A. K., Bhat, M. K. & Rao, C. P. (2012) Cu(II) complexes of glyco-imino-aromatic conjugates in DNA binding, plasmid cleavage and cell cytotoxicity, *J Chem Sci.* **124**, 1217-1228.
25. Rao, M. R., Gayatri, G., Kumar, A., Sastry, G. N. & Ravikanth, M. (2009) Cyclotriphosphazene ring as a platform for multiporphyrin assemblies, *Chemistry.* **15**, 3488-3496.
26. Bhattacharjya, S. & Ramamoorthy, A. (2009) Multifunctional host defense peptides: functional and mechanistic insights from NMR structures of potent antimicrobial peptides, *FEBS J.* **276**, 6465-6473.
27. Seefeldt, A. C., Nguyen, F., Antunes, S., Perebaskine, N., Graf, M., Arenz, S., Inampudi, K. K., Douat, C., Guichard, G., Wilson, D. N. & Innis, C. A. (2015) The proline-rich antimicrobial peptide Onc112 inhibits translation by blocking and destabilizing the initiation complex, *Nat Struct Mol Biol.* **22**, 470-475.
28. Silver, L. L. (2011) Challenges of antibacterial discovery, *Clinical microbiology reviews.* **24**, 71-109.
29. Kumar, A. & Balbach, J. (2017) Targeting the molecular chaperone SlyD to inhibit bacterial growth with a small molecule, *Sci Rep.* **7**, 42141.
30. Kumar, A. (2017) A small-molecule acts as a 'roadblock' on DNA, hampering its fundamental processes, *J Inorg Biochem.* **176**, 134-139.
31. Zanier, K., Nomine, Y., Charbonnier, S., Ruhlmann, C., Schultz, P., Schweizer, J. & Trave, G. (2007) Formation of well-defined soluble aggregates upon fusion to MBP is a generic property of E6 proteins from various human papillomavirus species, *Protein Expr Purif.* **51**, 59-70.
32. Zanier, K., Ould M'hamed Ould Sidi, A., Boulade-Ladame, C., Rybin, V., Chappelle, A., Atkinson, A., Kieffer, B. & Trave, G. (2012) Solution structure analysis of the HPV16 E6

oncoprotein reveals a self-association mechanism required for E6-mediated degradation of p53, *Structure*. **20**, 604-617.

33. Filipe, V., Hawe, A. & Jiskoot, W. (2010) Critical evaluation of Nanoparticle Tracking Analysis (NTA) by NanoSight for the measurement of nanoparticles and protein aggregates, *Pharm Res*. **27**, 796-810.

34. Zilfou, J. T. & Lowe, S. W. (2009) Tumor suppressive functions of p53, *Cold Spring Harb Perspect Biol*. **1**, a001883.

35. Scheffner, M., Werness, B. A., Huibregtse, J. M., Levine, A. J. & Howley, P. M. (1990) The E6 oncoprotein encoded by human papillomavirus types 16 and 18 promotes the degradation of p53, *Cell*. **63**, 1129-1136.

36. Huibregtse, J. M., Scheffner, M. & Howley, P. M. (1993) Localization of the E6-AP regions that direct human papillomavirus E6 binding, association with p53, and ubiquitination of associated proteins, *Mol Cell Biol*. **13**, 4918-4927.

37. Scheffner, M., Nuber, U. & Huibregtse, J. M. (1995) Protein ubiquitination involving an E1-E2-E3 enzyme ubiquitin thioester cascade, *Nature*. **373**, 81-83.

38. Donaldson, L. W., Skrynnikov, N. R., Choy, W. Y., Muhandiram, D. R., Sarkar, B., Forman-Kay, J. D. & Kay, L. E. (2001) Structural characterization of proteins with an attached ATCUN motif by paramagnetic relaxation enhancement NMR spectroscopy, *J Am Chem Soc*. **123**, 9843-9847.

39. Clore, G. M. & Iwahara, J. (2009) Theory, practice, and applications of paramagnetic relaxation enhancement for the characterization of transient low-population states of biological macromolecules and their complexes, *Chem Rev*. **109**, 4108-4139.

40. Dinesh, D. C., Kovermann, M., Gopalswamy, M., Hellmuth, A., Calderon Villalobos, L. I., Lilie, H., Balbach, J. & Abel, S. (2015) Solution structure of the PsIAA4 oligomerization

domain reveals interaction modes for transcription factors in early auxin response, *Proc Natl Acad Sci USA*. **112**, 6230-6235.

41. Gopalswamy, M., Kumar, A., Adler, J., Baumann, M., Henze, M., Kumar, S. T., Fandrich, M., Scheidt, H. A., Huster, D. & Balbach, J. (2015) Structural characterization of amyloid fibrils from the human parathyroid hormone, *Biochim Biophys Acta*. **1854**, 249-257.

42. Glatt, S., Zabel, R., Vonkova, I., Kumar, A., Netz, D. J., Pierik, A. J., Rybin, V., Lill, R., Gavin, A. C., Balbach, J., Breunig, K. D. & Muller, C. W. (2015) Structure of the Kti11/Kti13 heterodimer and its double role in modifications of tRNA and eukaryotic elongation factor 2, *Structure*. **23**, 149-160.

43. Kumar, A., Gopalswamy, M., Wolf, A., Brockwell, D. J., Hatzfeld, M. & Balbach, J. (2018) Phosphorylation-induced unfolding regulates p19(INK4d) during the human cell cycle, *Proc Natl Acad Sci USA*. **115**, 3344-3349.

44. Harper, D. M. (2009) Currently approved prophylactic HPV vaccines, *Expert Rev Vaccines*. **8**, 1663-1679.

45. Harper, D. M. (2009) Current prophylactic HPV vaccines and gynecologic premalignancies, *Curr Opin Obstet Gynecol*. **21**, 457-464.

46. Marquez-Gutierrez, M. A., Benitez-Hess, M. L., DiPaolo, J. A. & Alvarez-Salas, L. M. (2007) Effect of combined antisense oligodeoxynucleotides directed against the human papillomavirus type 16 on cervical carcinoma cells, *Arch Med Res*. **38**, 730-738.

47. Niu, X. Y., Peng, Z. L., Duan, W. Q., Wang, H. & Wang, P. (2006) Inhibition of HPV 16 E6 oncogene expression by RNA interference in vitro and in vivo, *Int J Gynecol Cancer*. **16**, 743-751.

48. Wei, Q. (2005) Pitx2a binds to human papillomavirus type 18 E6 protein and inhibits E6-mediated P53 degradation in HeLa cells, *J Biol Chem*. **280**, 37790-37797.

49. Butz, K., Denk, C., Ullmann, A., Scheffner, M. & Hoppe-Seyler, F. (2000) Induction of apoptosis in human papillomaviruspositive cancer cells by peptide aptamers targeting the viral E6 oncoprotein, *Proc Natl Acad Sci USA*. **97**, 6693-6697.
50. Liu, Y., Liu, Z., Androphy, E., Chen, J. & Baleja, J. D. (2004) Design and characterization of helical peptides that inhibit the E6 protein of papillomavirus, *Biochemistry*. **43**, 7421-7431.
51. Griffin, H., Elston, R., Jackson, D., Ansell, K., Coleman, M., Winter, G. & Doorbar, J. (2006) Inhibition of papillomavirus protein function in cervical cancer cells by intrabody targeting, *J Mol Biol*. **355**, 360-378.
52. Ramirez, J., Poirson, J., Foltz, C., Chebaro, Y., Sch rapp, M., Meyer, A., Bonetta, A., Forster, A., Jacob, Y., Masson, M., Deryckere, F. & Trave, G. (2015) Targeting the Two Oncogenic Functional Sites of the HPV E6 Oncoprotein with a High-Affinity Bivalent Ligand, *Angew Chem Int Ed Engl*. **54**, 7958-7962.
53. Hassan, P. A., Rana, S. & Verma, G. (2015) Making sense of Brownian motion: colloid characterization by dynamic light scattering, *Langmuir : the ACS journal of surfaces and colloids*. **31**, 3-12.
54. Roger, V., Cottet, H. & Cipelletti, L. (2016) A New Robust Estimator of Polydispersity from Dynamic Light Scattering Data, *Anal Chem*. **88**, 2630-2636.

## Figures legends

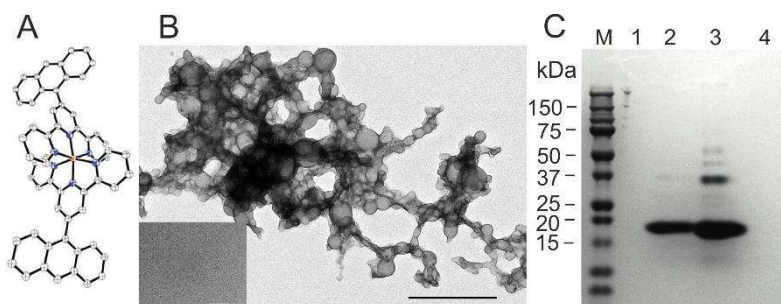


**Figure 1:**  $\text{Cu}^{2+}$  complex-induced aggregation of E6 F47R 4C/4S. (A) Molecular structure of the  $\text{Cu}^{2+}$  anthracenyl-terpyridine complex. (B) Transmission electron microscopy image of E6 F47R 4C/4S co-incubated with the  $\text{Cu}^{2+}$  complex. Inset in (B) shows E6 F47R 4C/4S before incubation. These grids were prepared at the 6 h time point. Scale bar represents 500 nm. (C) Analysis of E6 F47R 4C/4S aggregation by 12% SDS-PAGE. M – molecular weight marker, 1 – pellet of E6 F47R 4C/4S incubated with  $\text{Cu}^{2+}$ -perchlorate, 2 – untreated E6 F47R 4C/4S, 3 – pellet of E6 F47R 4C/4S incubated with  $\text{Cu}^{2+}$  complex and 4 – pellet of E6 F47R 4C/4S incubated with 9-anthracene methanol. These samples were prepared after 6 h of co-incubation. The position of the asterisk indicates monomeric E6 F47R 4C/4S.

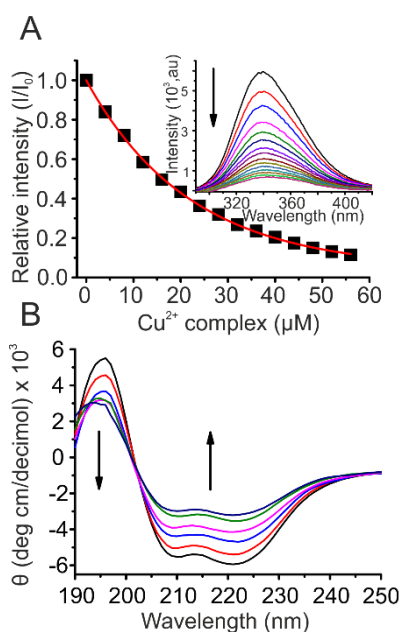


**Figure 2:** Interactions of  $\text{Cu}^{2+}$  complex with E6 F47R 4C/4S. (A) Fluorescence detected binding at 338 nm. Inset: spectral traces obtained during the titration experiment (see text). (B) Conformational changes in E6 F47R 4C/4S upon  $\text{Cu}^{2+}$  complex addition. In (A) and (B) black spectra corresponds to unbound E6 F47R 4C/4S and red onwards after stepwise addition of the  $\text{Cu}^{2+}$  complex (denoted by direction of arrow).

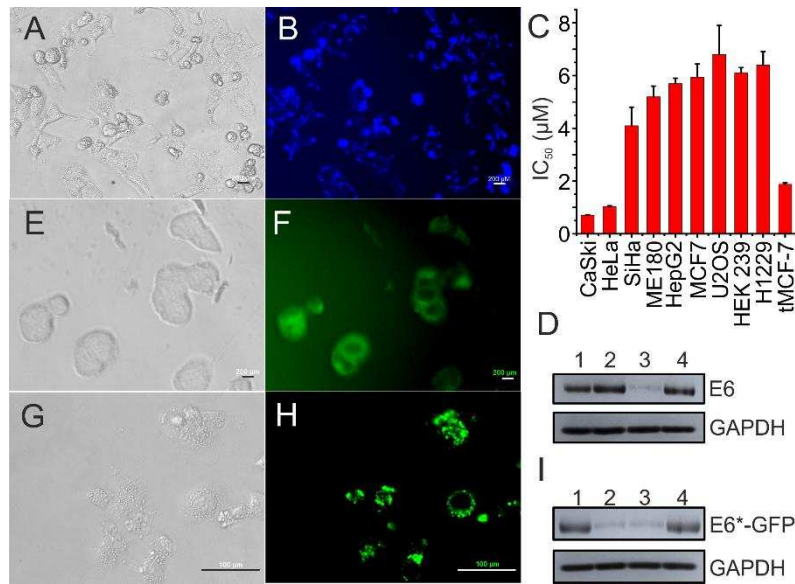


**Figure 3:** Cu<sup>2+</sup> complex induced aggregation of E6 inside cells. (A) Cu<sup>2+</sup> complex-treated HVP-infected HeLa cells showing the aggregation of E6 by phase contrast microscopy. (B) Fluorescence microscopy image of (A) under UV irradiation at 334 nm. (C) Half maximal inhibitory concentration (IC<sub>50</sub>, µM) plot for cells. Cell viability was determined using MTT assays. Error bars represent the mean of three independent experiment performed in triplicates. (D) Western blot analysis of E6. Lane – 1 and 2: control HeLa cells showing the presence of E6 in the soluble and cell pellet fractions, respectively; lane 3 and 4: Cu<sup>2+</sup> complex treated HeLa cells showing E6 in the soluble and insoluble fraction, respectively. (E) GFP-E6 F47R 4C/4S transfected MCF-7 cells imaged using phase contract microscopy. (F) Fluorescent image of (E) under excitation at 488 nm. (G) Cu<sup>2+</sup> complex treated transfected MCF-7 (tMCF-7) cells showing aggregation of GFP-E6 F47R 4C/4S using phase contrast microscopy. (H) Fluorescent image under excitation at 488 nm of (G) showing the aggregation of GFP-E6 F47R 4C/4S. Images in (B), (F) and (H) were pseudo-coloured using ImageJ software. (I) Western blot analysis of GFP-E6 F47R 4C/4S transiently expressed in MCF-7 cells. Lane – 1 and 2: cells showing GFP-E6 F47R 4C/4S expression in the soluble and cell pellet fraction, respectively. Lane 3 and 4: Cu<sup>2+</sup> complex treated transfected MCF-7 cells showing GFP-E6 F47R 4C/4S in

the soluble and insoluble fraction, respectively. In (D) and (I) GAPDH (Glyceraldehyde 3-phosphate dehydrogenase) was used as a loading control.

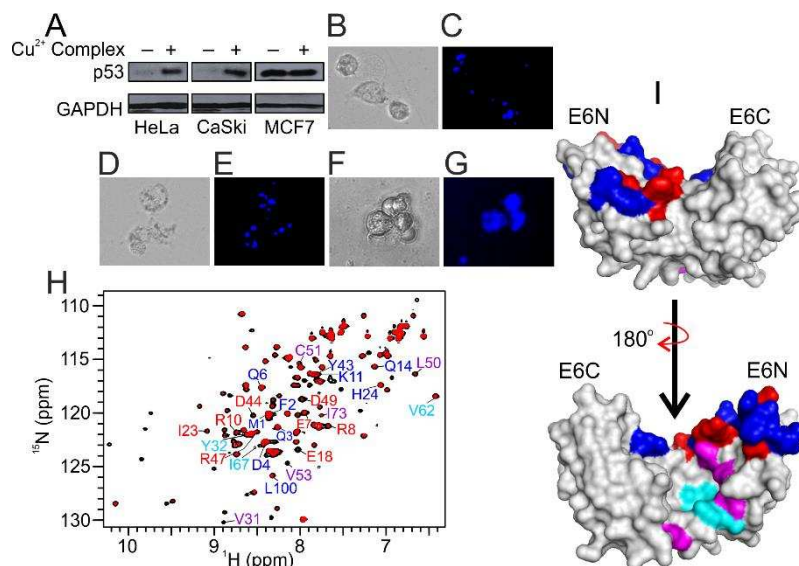


**Figure 4:** Relieving of the p53 hijacking mechanism by the  $\text{Cu}^{2+}$  complex. (A) Western blot analysis of p53 in the absence and presence of the  $\text{Cu}^{2+}$  complex in different cells. The cells were treated at  $\text{IC}_{50}$  values for 48 h. (B) – (G) Nuclear fragmentation of cells. (B) and (C) HeLa cells, (D) and (E) CaSki cells, (F) and (G) MCF-7. (B), (D) and (F) are phase contrast image and (C), (E) and (G) are fluorescence image of same. The cells were incubated with  $\text{Cu}^{2+}$  complex (HeLa and CaSki cells at  $1 \mu\text{M}$  and MCF-7 cells at  $6 \mu\text{M}$ ) for 48 h. The images were taken by exciting the cells with UV irradiation at 334 nm.  $\text{Cu}^{2+}$  complex auto-fluorescence was utilized for imaging. (H) NMR analysis showing an overlay of  $^1\text{H}$ - $^{15}\text{N}$  HSQC spectra of E6 F47R 4C/4S in the free-state (black) and bound to the  $\text{Cu}^{2+}$  complex (red). (I) NMR intensity analysis mapped onto the structure of E6 F47R 4C/4S (PDB code: 4XR8). Labelling in (H) and (I): residues which are assisting p53 binding are coloured blue. Residues assisting p53 binding and showing interaction with the  $\text{Cu}^{2+}$  complex (20 – 100 % reduction of NMR intensities) are shown in red. Cyan residues are involved in binding to the LxxLL motif of E6AP and magenta residues are involved in LxxLL binding and showing reduced NMR intensities (20 – 100 %).

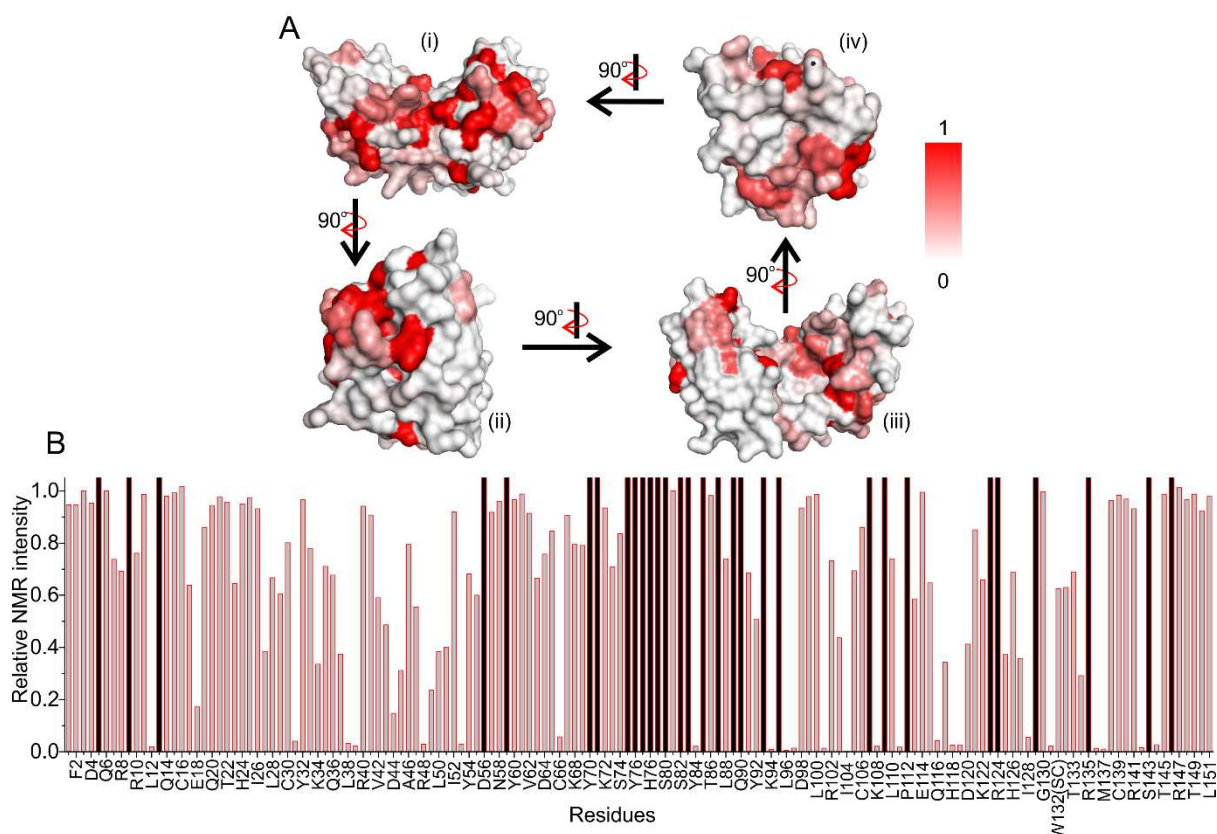


**Figure 5:** NMR analysis of the E6 F47R 4C/4S/Cu<sup>2+</sup> complex mapped onto the E6 structure (PDB:4XR8). (A) Colour coding follows the NMR intensity decreases (shown in (B)) upon Cu<sup>2+</sup> complex addition by a color gradient: red strongly affected and white not affected residues. (B) Relative NMR intensity analysis of the E6 F47R 4C/4S when bound to the Cu<sup>2+</sup> complex. Black filled bars are either prolines or residues which are not assigned and colored as white. Alternate residue labelling of the abscissa was used for clarity.